

# Relativistic hybrid stars with sequential first-order phase transitions and heavy-baryon envelopes

Jia Jie Li\*

*Institute for Theoretical Physics, J. W. Goethe University, D-60438 Frankfurt am Main, Germany*

Armen Sedrakian†

*Frankfurt Institute for Advanced Studies, D-60438 Frankfurt am Main, Germany and  
Institute of Theoretical Physics, University of Wrocław, 50-204 Wrocław, Poland*

Mark Alford‡

*Department of Physics, Washington University, St. Louis, Missouri 63130, USA  
(Dated: March 23, 2020)*

We compute the mass, radius and tidal deformability of stars containing phase transitions from hadronic to quark phase(s). These quantities are computed for three types of hadronic envelopes: purely nuclear, hyperonic, and  $\Delta$ -resonance–hyperon admixed matter. We consider either a single first-order phase transition to a quark phase with a maximally stiff equation of state (EOS) or two sequential first-order phase transitions mimicking a transition from hadronic (H) to a quark matter phase followed by a second phase transition to another quark phase. Such a construct emulates the results of the computations of the EOS which include 2SC and CFL color superconducting phases at low and high density. We explore the parameter space which produces low-mass twin and triplet configurations where equal-mass stars have substantially different radii and tidal deformabilities. We demonstrate that while for purely hadronic stiff EOS the obtained maximum mass is inconsistent with the upper limit on this quantity placed by GW170817, the inclusion of the hyperonic and  $\Delta$ -resonance degrees of freedom, as well as the deconfinement phase transition at sufficiently low density, produces a configuration of stars consistent with this limit. The obtained hybrid star configurations are in the mass range relevant for the interpretation of the GW170817 event. We compare our results for the tidal deformability with the limits inferred from GW170817 showing that the onset of non-nucleonic phases, such as  $\Delta$ -resonance–hyperon admixed phase and/or the quark phase(s), are favored by these data if the nuclear EOS is stiff. Also, we show that low-mass twins and especially triplets proliferate the number of combinations of possible types of stars that can undergo a merger event, the maximal number being six in the case of triplets. The prospects for uncovering the first-order phase transition(s) to and in quark matter via measurements of tidal deformabilities in merger events are discussed.

## I. INTRODUCTION

The first multimessenger observations of gravitational waves (GW) by the LIGO-Virgo Collaboration from the binary neutron star merger event GW170817 [1–3] have provided important new constraints on the equation of state (EOS) of dense matter through the measurement of the tidal deformabilities and masses of neutron stars involved. The combination of these results with the recent measurement of the highest mass of a millisecond pulsar,  $M = 2.14^{+0.10}_{-0.09} M_{\odot}$  (within a 68.3% credibility interval) for pulsar PSR J0740+6620 [4], provides the most stringent astrophysical constraints to date on the properties of ultra-dense matter. To be consistent with these data, the EOS of the dense matter must be moderately soft at intermediate densities to allow for relatively small tidal deformabilities but it must be hard enough at high densities to allow for two-solar-mass neutron stars.

Constraints on the EOS of dense matter were placed also using the pulse-profile modeling of the isolated 205.53 Hz

millisecond pulsar PSR J0030+0451 observed in x-rays by the Neutron Star Interior Composition Explorer (NICER) experiment. The two independent analysis, which used different emitting spot models, constrained the mass and equatorial radius of this object within a 68.3% credibility interval to  $1.34^{+0.15}_{-0.16} M_{\odot}$  and  $12.71^{+1.14}_{-1.19}$  km [5] and  $1.44^{+0.15}_{-0.14} M_{\odot}$  and  $13.02^{+1.24}_{-1.06}$  km [6].

The actual composition of matter in the interior of neutron stars remains unclear. One possibility is a deconfinement phase transition from bound hadronic states to liberated quark states (see, for instance, Refs. [7–10] and references therein). The effect of a *strong first-order* phase transition on tidal deformabilities of the neutron star in the context of the GW170817 event has been explored by a number of groups [11–22] showing that the hadron-quark phase transition at low enough density,  $\rho \simeq 2\text{--}3\rho_0$ , where  $\rho_0$  is the nuclear saturation density, relaxes the tension between the inferred tidal deformabilities and those predicted by purely hadronic models without a phase transition. Of particular interest in this context is the emergence of *twin* stars, where purely nucleonic and hybrid stars have the same masses, but different radii [12].

The onset in dense matter of heavy baryonic states, such as hyperons and  $\Delta$ -resonances, was explored in Refs. [23, 24], taking into account the data from GW170817. These works showed that the EOS, in this case, can be hard enough to sup-

\* jiajeli@itp.uni-frankfurt.de

† sedrakian@fias.uni-frankfurt.de

‡ alford@physics.wustl.edu

port two-solar-mass neutron stars and that  $\Delta$ -resonances allow for intermediate-density-range softening of the EOS, which is in line with the low values of deformabilities inferred for  $M \simeq 1.4M_{\odot}$  stars. However, the matter containing heavy baryonic states may undergo a phase transition to quark matter at densities relevant for compact stars. Therefore, phenomenologically, it is of great interest to study a sequence of phase transitions, where the purely nucleonic matter undergoes a phase transition to matter with heavy baryon states (hyperons and  $\Delta$ -resonances) at a density somewhat above the nuclear saturation density which is followed by deconfinement of hadrons to quarks at some higher density. Below, for the sake of brevity, the conglomerate of hadronic phases of a hybrid star, which surrounds its quark core is referred as *hadronic envelope*.

Thus, the first motivation of this work is to study the tidal deformabilities of a neutron star with such a sequence of phase transitions. The second motivation of this work is to compute the tidal deformabilities of hybrid stars with sequential first-order phase transitions [25]. For example, this scenario can be realized if with increasing density the hadronic matter makes a transition to an intermediate-density quark phase “Q1” [e.g., the two-flavor color-superconducting (2SC) quark phase [26]], followed by a second transition to a higher-density quark phase “Q2” [e.g., the three-flavor color-flavor-locked (CFL) quark phase [27]]. Although we are concerned with the phenomenological description of such phase transition, Nambu-Jona-Lasinio (NJL) model-based computations [28] confirm the possibility of such an outcome if a repulsive vector interaction is added to the standard NJL Lagrangian.

In this work we explore the regime where the phase transitions take place at low enough density so that low-mass stars with  $M \simeq 1.4M_{\odot}$  may contain quark matter. It has been shown in Ref. [25] that sequential phase transition may lead to the appearance of *triplet configurations* with three stars having the same mass but different radii. If realized, such a possibility will lead to a proliferation of the possible combinations of stars that could have been involved in the GW170817 event. This extends the study of Ref. [12] where the tidal deformabilities of *twin configurations* have been analyzed.

This paper is organized as follows. In Sec. II we briefly define the EOS that we use to describe the hadronic and quark phases. In Sec. III we present the results for tidal deformabilities of spherically symmetric stellar configurations and in Sec. IV we confront them with the inferences from GW170817 and NICER observations of PSR J0030+0451. Our conclusions are given in Sec. V.

## II. CONSTRUCTION OF EOS

### A. Hadronic EOS

To assess how our results depend on the hadronic matter EOS used to describe low-density matter, we employ three representative EOS which feature different hadronic compositions: (i) a purely nucleonic EOS calculated from the DD-

ME2 functional [29], as used in Ref. [25], which is stiff in the entire relevant density range; (ii) a hyperonic EOS, based on an extended version of the DD-ME2 functional that includes hyperons, which is softer than the nucleonic one at densities  $\rho/\rho_0 \gtrsim 2.5$  [30]; and (iii) a hyperon- $\Delta$  admixed matter EOS [30], which is soft at low densities ( $1.5 \lesssim \rho/\rho_0 \lesssim 3.0$ ) but is stiff at high densities ( $\rho/\rho_0 > 3.0$ ). The tabulated EOS are provided in Table I.

### B. Quark matter EOS

To model the EOS of the quark phase(s) we employ a *synthetic* constant-sound-speed (CSS) approach [31, 32]. We assume a first-order phase transition manifested as a sharp boundary between the phases, which is the case when mixed phases are disfavored by surface tension and electrostatic energy costs [33, 34]. Here we use the extension of CSS EOS to

TABLE I. EOS of hadronic matter used to model hybrid stars. The first column lists the density  $\rho$  in units of  $\text{fm}^{-3}$ . The columns correspond to  $\epsilon - p$  relation for purely nucleonic ( $N$ ), hyperonic ( $NY$ ) and hyperon- $\Delta$  admixed ( $NY\Delta$ ) matter. These are given in units of  $\text{MeV fm}^{-3}$ .

$\rho$	$N$		$NY$		$NY\Delta$	
	$\epsilon$	$p$	$\epsilon$	$p$	$\epsilon$	$p$
0.072	68.20	0.41				
0.100	94.94	0.80				
0.125	118.93	1.36				
0.150	143.07	2.26				
0.175	167.40	3.76				
0.200	192.00	6.07				
0.225	216.95	9.44			216.92	8.19
0.250	242.33	14.04			241.94	8.45
0.275	268.25	20.05			267.04	9.97
0.300	294.78	27.57			292.36	13.37
0.325	322.00	36.66			318.04	18.94
0.350	349.98	47.34	349.97	46.40	344.24	26.74
0.375	378.78	59.63	378.57	54.73	371.08	36.71
0.400	408.45	73.50	407.69	61.72	398.64	48.33
0.425	439.04	88.93	437.24	68.48	426.93	59.63
0.450	470.57	105.87	467.19	75.64	455.87	70.62
0.475	503.09	124.29	497.55	83.28	485.43	82.19
0.500	536.62	144.16	528.33	91.43	515.63	94.43
0.550	606.78	188.07	591.16	109.37	577.91	120.92
0.600	681.17	237.36	655.72	129.67	642.72	149.68
0.650	759.89	291.80	722.08	152.49	710.02	179.42
0.700	842.99	351.22	790.29	177.97	779.46	205.85
0.750	930.50	415.47	860.42	206.16	850.83	233.39
0.800	1022.46	484.46	932.51	237.01	924.03	260.04
0.850	1118.87	558.09	1006.62	269.83	998.87	286.30
0.900	1219.75	636.29	1082.57	299.70	1075.30	313.72
0.950	1325.10	719.01	1160.18	330.14	1153.28	342.73
1.000	1434.92	806.21	1239.44	362.05	1232.85	373.58

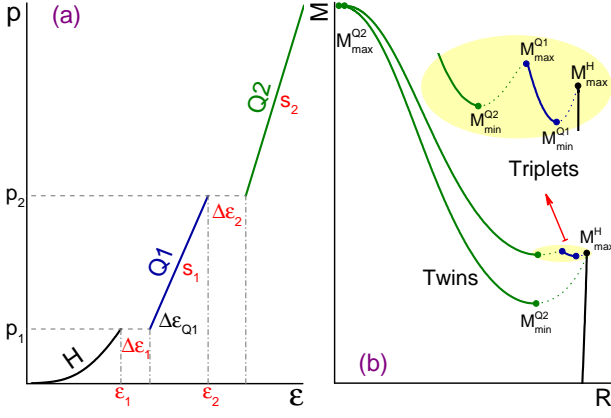


FIG. 1. Schematic plot showing the parametrizations of the equation of state with two phase transitions (a) and the resultant mass-radius relation (b).

the case of two sequential phase transitions by writing [25]

$$p(\varepsilon) = \begin{cases} p_1, & \varepsilon < \varepsilon < \varepsilon_1 + \Delta\varepsilon_1 \\ p_1 + s_1[\varepsilon - (\varepsilon_1 + \Delta\varepsilon_1)], & \varepsilon_1 + \Delta\varepsilon_1 < \varepsilon < \varepsilon_2 \\ p_2, & \varepsilon_2 < \varepsilon < \varepsilon_2 + \Delta\varepsilon_2 \\ p_2 + s_2[\varepsilon - (\varepsilon_2 + \Delta\varepsilon_2)], & \varepsilon > \varepsilon_2 + \Delta\varepsilon_2, \end{cases} \quad (1)$$

where  $p$  is the pressure and  $\varepsilon$  is the energy density. The first phase transition from hadronic to quark matter takes place at  $\varepsilon_1, p_1$ . The second phase transition within the quark phase, from Q1 to Q2 (e.g. from the 2SC to CFL color superconducting phase), takes place at  $\varepsilon_2, p_2$ ;  $s_1$  and  $s_2$  are squared sound speeds in phases 1 and 2. If the energy density at the center of a star is  $\varepsilon_c < \varepsilon_2$ , there is only a single phase transition in that star. If  $\varepsilon_c > \varepsilon_2$  then two phase transitions take place within the star.

Figure 1 (a) schematically illustrates the parameterization (1) in the case of double phase transitions; here H refers to the hadronic phase, Q1, and Q2 to quark phases. There are, in total, six independent parameters [25], all of which enter Eq. (1)

$$\varepsilon_1, \Delta\varepsilon_1, \varepsilon_2, \Delta\varepsilon_2, s_1, s_2. \quad (2)$$

Instead of  $\varepsilon_2$  it is convenient to use the energy-density width of the Q1 phase,  $\Delta\varepsilon_{Q1}$ . A characteristic mass-radius (MR) relation that results from solving the Tolman-Oppenheimer-Volkoff equations with the EOS (1) as an input is shown in Fig. 1 (b). We illustrate an EOS with parameters chosen so that twins or triplets of stars arise, where each new phase of matter introduces a new family of compact stars. It is convenient for further discussion to define maximal masses for the branches, labeled by the phase occurring at the center of the stars in that branch,

$$M_{\max}^H, M_{\max}^{Q1}, M_{\max}^{Q2}.$$

In addition we define the minimum values of the masses of the stellar branches associated with the quark phases,

$$M_{\min}^{Q1}, M_{\min}^{Q2}.$$

For a large jump in energy density  $\Delta\varepsilon_1$ , when the central pressure of a star rises above  $p_1$  and Q1 quark matter appears in the core, the star could become unstable immediately [dashed line in Fig. 1 (b)]. However, it is possible to regain stability at higher central pressure (solid line), resulting in a *second stable branch* (or the ‘‘third family’’ of compact stars) if the parameters  $p_1, \Delta\varepsilon_1$  and  $s_1$  are chosen appropriately. In particular, in this case, twin configurations appear where two stars have the same masses but different radii [12, 17–20]. If a second phase transition in the quark phase takes place, then a *third stable branch* (or fourth family) of compact stars containing Q2 quark matter in the core arises. For some choice of parameters *triplet configurations* can arise [25] where three stars have the same masses but different radii.

To study the possible role of quark phases in the merger event GW170817, we select from the multitude of equilibrium solutions for the stellar configurations generated by the six-dimensional parameter space (2) those that correspond to low-mass configurations with one or two quark phases. First, we require the maximum mass, for stars with the densest quark phase at their center, to reach  $2M_\odot$  to be compatible with Shapiro delay measurements [35–37],

$$M_{\max}^{Q2} = 2.0M_\odot, \quad (\text{single/double phase transition}), \quad (3)$$

where, in the case of a single phase transition, it is assumed that the transition takes place directly from the hadronic phase to the Q2 quark phase. To restrict the parameter space further in the case of a double phase transition, we impose the following conditions

$$M_{\max}^H = M_{\max}^{Q1}, \quad M_{\min}^{Q1} = M_{\min}^{Q2}, \quad (\text{double phase transition}), \quad (4)$$

a construction that guarantees that if a twin of hadronic star arises due to the phase transition to the Q1 phase, the emergence of the new branch due to the Q2 phase replicates for the triplet the mass range covered by the twin. Thus, the range of mass twins is automatically extended to the mass triplets.

Finally, we set  $s_1 = 0.7$  and  $s_2 = 1.0$  as in Ref. [25]. With these constraints we now have a 1-parameter family of stars: if we specify the value of  $M_{\max}^H$  (which is equivalent to specifying  $\varepsilon_1$ ), all the remaining parameters of the problem (i.e.,  $\Delta\varepsilon_1, \Delta\varepsilon_{Q1}$  and  $\Delta\varepsilon_2$ ) are determined by the conditions (3) and (4). Note that the condition  $M_{\max}^{Q2} > M_{\max}^H$  is an *assumption*; i.e., we require the maximum mass configuration to occur on the Q2 branch. In the case of a single phase transition, our discussion is complementary to those given in Refs. [12, 13, 16–21], but we take into account the possibility of various compositions of the hadronic phases surrounding the quark matter core of a hybrid star, i.e., the hadronic envelope of the star.

### III. MASS, RADIUS AND DEFORMABILITY

#### A. Single phase transition

We start the discussion with the simpler case of hybrid stars with a single phase transition, varying the composition

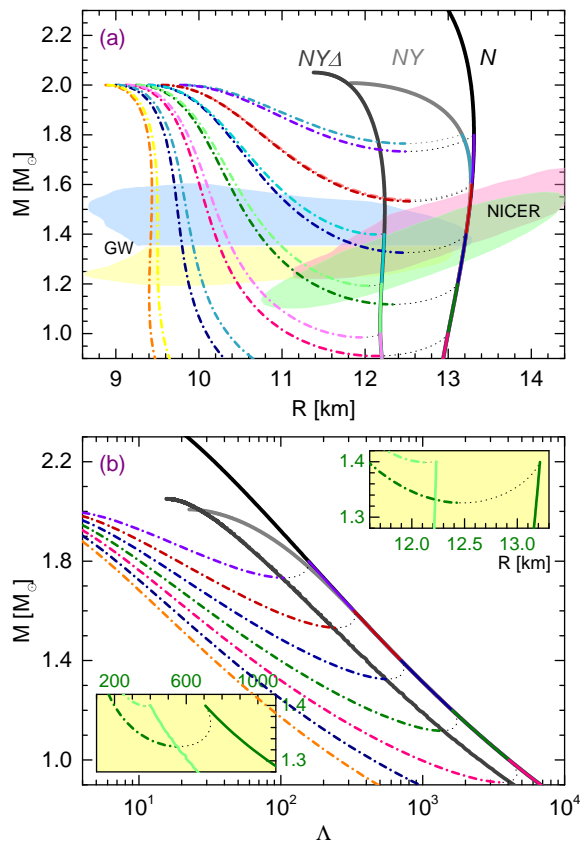


FIG. 2. (a) Mass-radius relation for hybrid stars with a single phase transition, with three different hadronic envelopes: nucleonic ( $N$ ), hyperonic ( $NY$ ) and  $\Delta$ -resonance–hyperon admixed ( $NY\Delta$ ). Each hybrid star branch bifurcates from a hadronic sequence at a point which corresponds to the maximum value of the mass of the respective hadronic branch  $M_{\text{max}}^{\text{H}}/M_{\odot}$ . The figure displays hybrid configurations which correspond to  $M_{\text{max}}^{\text{H}}/M_{\odot} = 0.60$ - $1.80$ . Note that the hyperons appear only in the two sequences with  $M_{\text{max}}^{\text{H}}/M_{\odot} = 1.60$  and  $1.80$ . In each case the maximum mass of the hybrid branch is fixed at  $M_{\text{max}}^{\text{Q}2}/M_{\odot} = 2.00$ . The dotted lines indicate unstable configurations. The shading represents the 90% posterior credible range of masses and radii for the two stars that merged in the GW170817 event [38], and the 68% posterior probability of mass-radius for the millisecond pulsar PSR J0030+0451 obtained by using NICER data [5, 6]. (b) Mass-deformability relation for the configurations shown in (a). We show only the hybrid star configurations that have  $N$  envelopes for the sake of clarity. The insets show the results for the case  $M_{\text{max}}^{\text{H}}/M_{\odot} = 1.40$ . The smaller radius (deformability) curve corresponds to  $NY\Delta$  envelope stars, whereas the larger ones correspond to  $N$  envelope stars.

of the hadronic envelope. As explained above, our strategy is to vary the value of  $M_{\text{max}}^{\text{H}}$  while keeping  $M_{\text{max}}^{\text{Q}2}/M_{\odot} = 2.00$  fixed. The latter condition fully determines the energy density jump at the first-order phase transition. The solutions of Tolman-Oppenheimer-Volkoff equations are shown in Fig. 2 in the form of MR and mass-deformability (MA) relations.

It is seen that the onset of hyperons ensures that the maximum masses of the hadronic sequences stay close to  $2M_{\odot}$ , whereas the maximum mass of the pure nucleonic EOS has a

much higher value,  $2.48M_{\odot}$ . Thus, the hyperonic sequences are consistent with the *upper limit* on the maximum mass inferred from the analysis of GW170817 [39–42], whereas their nucleonic counterparts are not. Note, however, that if a phase transition to quark matter occurs, then the maximum mass of the purely hadronic branch is not physically relevant. Otherwise, there are no significant differences between the hyperonic and purely nucleonic branches of compact stars. The inclusion of  $\Delta$ -particles shrinks the radius by about 1 km as expected [23, 30], without affecting other features of the MR diagram. The minimum mass on the hybrid star branch moves to a higher value with the onset of heavy baryons by less than 10% of mass.

A more quantitative analysis is provided by Table II where the transition density, the magnitude of the jump in energy density at the transition, and the range of masses where twins appear are shown. This reveals the inverse correlation between the magnitude of the jump and transition density: the larger the transition density, the smaller the jump needed to achieve the  $2M_{\odot}$  limit for the hybrid star branch. The range of masses where twin configurations exist also decreases with the increase of the transition density, which is the natural consequence of the shape of the MR curves. We also note that the onset of heavy baryons suppresses the range of masses over which twin configurations exist.

The mass-deformability relations for the stars with nucleonic matter envelopes are shown in Fig. 2 (b). The results for EOS with a hyperonic matter envelope or a hyperon- $\Delta$  admixed matter envelope are not shown, as they are very close to their nucleonic counterparts. The key effect of the onset of the quark matter is to reduce the tidal deformability of the star of a given gravitational mass, a fact also established in Refs. [12, 19]. The reduction is seen in the lower inset of

TABLE II. Parameters for the EOS that feature different hadronic envelopes, supporting  $M_{\text{max}}^{\text{Q}2}/M_{\odot} = 2.00$ . The EOS are identified by the maximum mass of the hadronic branch  $M_{\text{max}}^{\text{H}}/M_{\odot} = 0.60$ - $1.80$ , in steps of  $0.20$ . The energy density at the transition point  $\varepsilon_1$  is in units of  $\text{MeV fm}^{-3}$ . The last column lists the mass ranges for twin configurations.

Had.	$M_{\text{max}}^{\text{H}}$	$\rho_{\text{tr}}/\rho_0$	$\varepsilon_1$	$\Delta\varepsilon_1/\varepsilon_1$	$\Delta M_{\text{twin}}$
$N$	0.600	1.555	228.431	1.813	0.095
	0.800	1.734	256.308	1.542	0.095
	1.000	1.901	283.025	1.344	0.090
	1.200	2.069	310.423	1.187	0.082
	1.400	2.245	340.084	1.057	0.074
	1.600	2.439	373.763	0.949	0.067
$NY$	1.800	2.665	414.552	0.859	0.065
	1.600	2.549	393.077	0.857	0.062
	1.800	3.226	516.463	0.527	0.035
$NY\Delta$	0.600	2.011	298.133	1.168	0.093
	0.800	2.259	337.195	0.961	0.026
	1.000	2.448	367.971	0.844	0.015
	1.200	2.634	399.029	0.755	0.008
	1.400	2.881	441.724	0.653	0.001



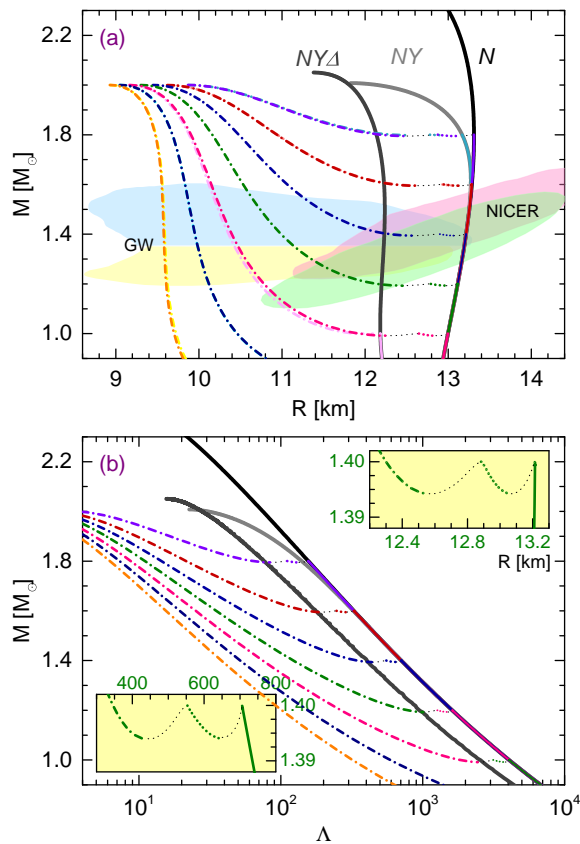


FIG. 3. The same as in Fig. 2, but in the case of quark matter EOS with sequential phase transitions. The insets show the results for MR and  $M\Lambda$  in the case of  $M_{\max}^H/M_{\odot} = 1.40$ . The emergence of low-mass triplets in this case is clearly visible.

Fig. 2 (b). This decrease is large enough (several hundreds) that hadronic stars and hybrid stars will be distinguishable in binary compact star mergers. Thus, if the masses of the individual stars are measured, their deformabilities will allow distinguishing between the hadronic and hybrid stars for a chosen (plausible) hadronic EOS. The tidal deformability for a  $1.4M_{\odot}$  star  $\Lambda_{1.4}$  can be as low as  $\sim 50$ -100, corresponding to a radius of about  $\sim 9.5$ -10.5 km, in the extreme case where the phase transitions occur at densities below  $2\rho_0$ . Note, also, that there exists a minimum mass for neutron star configurations when these are formed in core-collapse supernovae which is of the order of  $1.0M_{\odot}$  [43, 44].

### B. Two sequential phase transitions

Next, we turn to the results found in the case of two sequential phase transitions. For fixed transitional mass  $M_{\max}^H$ , on one hand, triplet configurations occur if the discontinuities in energy density,  $\Delta\varepsilon_1$  and  $\Delta\varepsilon_2$ , are large enough to yield *separate* stable Q1- and Q2-branch solutions. On the other hand, in order to be compatible with the observational mass constraint ( $M_{\max}/M_{\odot} > 2$ ) these jumps have to be not too large in order for the hybrid branches to be stable. This restricts the

mass range for triplet configurations to a quite narrow range, as discussed below.

The MR relations for nonrotating stars in this case are shown in Fig. 3 (a). We observe that with  $M_{\max}^{Q2}/M_{\odot} = 2.00$ , for the stiff nucleonic EOS, it is possible to have triplet configurations to a large range of maximum masses on the hadronic branch  $M_{\max}^H/M_{\odot} \in [0.60 - 1.80]$ . The onset of hyperons softens the high-density domain of the EOS and affects only the high-mass domain of the MR diagram. Note that hyperons appear in compact stars with masses  $M/M_{\odot} \geq 1.5$  [45–47], but their effect on the mass of the star becomes sizable only for the most massive stars. The triplet configurations appear in this case for stars with masses above  $1.5M_{\odot}$ . The MR curves for stars having hyperonic or  $\Delta$ -containing envelopes are almost indistinguishable from their nucleonic counterparts. Once  $\Delta$ 's are allowed one finds a reduction in the radius of the stars, as already observed in the case of a single phase transition. As a consequence, for  $NY\Delta$  stars we only find triplets at very low mass ( $M/M_{\odot} \leq 1$ ) for which the configurations are unstable. We thus conclude that if the radii on the hadronic branch are small (in particular, the radius of the maximal-mass star on that branch,  $M_{\max}^H$ ), then the triplet solutions can exist either only in a narrow range of radii, or they are eliminated completely. Note that because of the lower mass limit for neutron stars, the stability of low-mass triplets is an issue.

A more quantitative insight into the results can be obtained from Table III. It is seen that the triplet solutions exist in a very narrow range of masses; the presence of heavy baryons suppresses this range even further. Note also that triplet configurations arise in the case of nucleonic stars, but are constrained in the case of hyperon- $\Delta$  admixed matter to very low values of masses  $M/M_{\odot} \leq 1$ . It may be concluded from Table III that stiffer hadronic equations of state can give rise to triplets for a wider range of transition densities.

TABLE III. Parameters for the EOS that with different hadronic envelopes, supporting  $M_{\max}^{Q2}/M_{\odot} = 2.00$ . The EOS are identified by the transition mass  $M_{\max}^H/M_{\odot} = 0.60$ -1.80, in steps of 0.20. The energy density at the transition point  $\varepsilon_1$  is in units of  $\text{MeV fm}^{-3}$ . The last column presents the mass ranges for triplet configurations.

Had.	$M_{\max}^H$	$\rho_{tr}/\rho_0$	$\varepsilon_1$	$\Delta\varepsilon_1/\varepsilon_1$	$\Delta\varepsilon_2/\varepsilon_1$	$\Delta\varepsilon_{Q1}/\varepsilon_1$	$\Delta M_{\text{triplet}}$
N	0.600	1.555	228.431	0.860	0.971	0.037	0.011
	0.800	1.734	256.308	0.808	0.755	0.042	0.010
	1.000	1.901	283.025	0.767	0.602	0.047	0.008
	1.200	2.069	310.423	0.731	0.484	0.054	0.007
	1.365	2.213	334.670	0.706	0.405	0.062	0.006
	1.400	2.245	340.084	0.700	0.399	0.064	0.006
NY	1.600	2.439	373.763	0.665	0.328	0.078	0.005
	1.800	2.665	414.552	0.630	0.292	0.109	0.005
NY	1.600	2.549	393.077	0.604	0.294	0.075	0.004
	1.800	3.226	516.463	0.410	0.158	0.085	0.002
NY $\Delta$	0.600	2.011	298.133	0.658	0.522	0.026	0.004
	0.800	2.259	337.195	0.682	0.287	0.022	0.002
	1.000	2.448	367.971	0.679	0.173	0.021	0.001

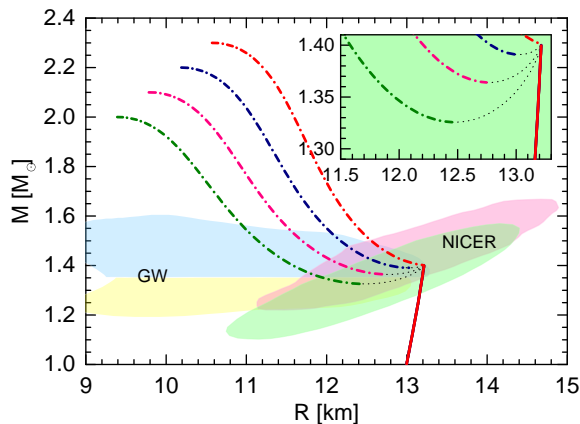


FIG. 4. Mass-radius relation for hybrid EOS with a single phase transition and nucleonic envelope. The EOS are identified by the maximum mass  $M_{\max}^{\text{Q}^2}/M_{\odot} = 2.00\text{-}2.30$ , and the maximum mass of the hadronic star, which is fixed at  $M_{\max}^{\text{H}}/M_{\odot} = 1.40$ . The shading is the same as in Fig. 2. The emergence of twin configurations is shown in the inset.

The mass-deformability relations for the configurations discussed above are shown in Fig. 3 (b) in the case of nucleonic matter envelopes. The results in the cases of hyperonic envelopes or hyperon- $\Delta$  admixed envelopes are not shown, as they are very close to their nucleonic counterparts. However, it should be kept in mind that in the case of hypernuclear envelopes the triplet configurations appear in the high-mass range and the deformabilities are small. In the case of hyperon- $\Delta$  admixed envelopes the reduction of the radius leads to the restriction to very low masses; in this case, their tidal deformabilities are large. We again see in Fig. 3 (b) that the phase transition leads to a reduction of tidal deformability; i.e., the  $\Lambda$  value is smaller for hybrid stars as compared to the same mass nucleonic stars [see also the lower inset in Fig. 3 (b)]. As in the case of a single phase transition, this decrease is quantitatively large enough, and the prospects of discrimination between hadronic and hybrid configurations remain intact. In this case, however, the situation is more complex as there are pairs of hybrid stars with the same mass. This leads to a proliferation of the sorts of stars that can take part in a merger; these issues will be discussed below.

### C. Varying $M_{\max}^{\text{Q}^2}$

So far we have kept the value  $M_{\max}^{\text{Q}^2}/M_{\odot} = 2.00$  fixed. This was in part motivated by the recent arguments which place the maximum mass of a neutron star in a narrow range slightly above this value. First, the analysis of the GW170817 event by several groups suggests an approximate *upper limit* on the maximum mass of a neutron star [39–42]. References [39–41] combined gravitational-wave and electromagnetic signals with numerical relativity simulations to limit the maximum mass to the range  $2.15\text{-}2.30M_{\odot}$ . The quasiuniversal relations that describe neutron stars and models of kilonovae were used to draw a similar bound on the maximum mass in Ref. [42].

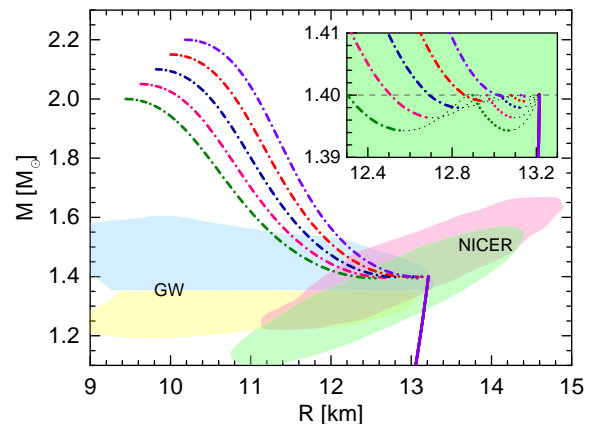


FIG. 5. The same as in Fig. 4, but calculated with hybrid EOS with two sequential phase transitions. The inset illustrates the emergence of triplet configurations.

As mentioned in the Introduction, a direct astrophysical *lower bound*  $2.14^{+0.10}_{-0.09}M_{\odot}$  (68.3% credibility interval) on the maximum mass of a neutron star was recently obtained via combination of the Shapiro delay data taken over 12.5 yr at the NANOGrav with orbital-phase-specific observations using the Green Bank Telescope from the mass measurement of the millisecond pulsar PSR J0740+6620 [4]. Combining the lower and upper bounds quoted above, one concludes that the maximum mass of a neutron star is located in the band  $2.15\text{-}2.30M_{\odot}$ .

We next explore the sensitivity of our results towards varying the value of  $M_{\max}^{\text{Q}^2}$  in the cases of single and two sequential phase transitions. To this end, we have fixed the value of  $M_{\max}^{\text{H}}/M_{\odot} = 1.40$  and imposed again the conditions (4) adapted for the cases of double phase transition.

The effects of varying  $M_{\max}^{\text{Q}^2}$  on the MR relations are shown in Fig. 4 for a single phase transition and in Fig. 5 for two sequential phase transitions. We observe that a larger maximum mass leads to smaller ranges of radii (and masses) where twin and triplet solutions exist. This effect is illustrated more quantitatively in Tables IV and V where additional parameters fully characterizing the EOS are given.

TABLE IV. Parameters for the EOS with  $M_{\max}^{\text{H}} = 1.40$ . The EOS are identified by the maximum mass  $M_{\max}^{\text{Q}^2}/M_{\odot} = 2.00\text{-}2.30$ , in steps of 0.10. The energy density at transition point  $\varepsilon_1$  is  $340.084 \text{ MeV fm}^{-3}$ . The last column presents the mass ranges for twin configurations.

Had.	$M_{\max}^{\text{Q}^2}$	$\Delta\varepsilon_1/\varepsilon_1$	$\Delta M_{\text{twin}}$
N	2.000	1.057	0.074
	2.100	0.878	0.036
	2.200	0.721	0.009
	2.300	0.583	0.000

TABLE V. Parameters for the EOS with  $M_{\max}^{\text{H}} = 1.40$ . The EOS are identified by the maximum mass  $M_{\max}^{\text{Q}2}/M_{\odot} = 2.00\text{-}2.20$ , in steps of 0.05. The energy density at transition point  $\varepsilon_1$  is  $340.084 \text{ MeV fm}^{-3}$ . The last column presents the mass ranges for triplet configurations.

Had.	$M_{\max}^{\text{Q}2}$	$\Delta\varepsilon_1/\varepsilon_1$	$\Delta\varepsilon_2/\varepsilon_1$	$\Delta\varepsilon_{\text{Q}1}/\varepsilon_1$	$\Delta M_{\text{triplet}}$
	2.000	0.700	0.392	0.064	0.006
	2.050	0.681	0.309	0.053	0.004
$N$	2.100	0.665	0.232	0.042	0.002
	2.150	0.652	0.158	0.033	0.001
	2.200	0.642	0.088	0.025	0.000

#### IV. COMPARISON WITH THE DATA FROM GW170817 EVENT

We now confront the tidal deformabilities of our neutron star models with the observational constraints for this quantity obtained from the analysis of the GW170817 event. We assume the chirp mass  $\mathcal{M} = 1.186M_{\odot}$  and compare only with the analysis which assumes the (more plausible) low-spin case [38]. Figure 6 displays the tidal deformabilities  $\Lambda_1$  and  $\Lambda_2$  of the stars involved in the binary with masses  $M_1$  and  $M_2$  in the case of a single phase transition. In panel (a) the hybrid EOS for the binary are identified by the value of  $M_{\max}^{\text{H}}$ . In panel (b) we fix this value at  $1.40M_{\odot}$ , which is close to the experimentally inferred value in the case of equal-mass binary assumption. The same in the case of two sequential phase transitions is shown in Fig. 7. In these figures, the diagonal line corresponds to the case of an equal-mass binary with  $M_{1,2} = 1.362M_{\odot}$ . The shaded areas correspond to the 90% and 50% confidence limits, which are inferred from the analysis of the GW170817 event using the PhenomPNRT waveform model [48]. Note that the observational analysis depends on the assumed theoretical waveforms. For example, 90% confidence upper limits on tidal deformabilities predicted by the TaylorF2 model are larger by about 20% than those predicted by the PhenomRNRT model used in our figures.

It is seen that the largest values of the deformability in the  $\Lambda_1$ - $\Lambda_2$  plane are generated by the curve corresponding to the purely nucleonic EOS, as this is the hardest possible EOS in our collection of models. The case of hyperonic EOS is almost indistinguishable from the nucleonic one. The corresponding curves remain slightly outside the 90% credibility level set by the PhenomPNRT model ( $\sim 10\%$  for the equal-mass case). In the case where  $\Delta$ 's are included in the composition, the  $\Lambda$  values are significantly reduced in agreement with the previous result [23].

The fact that mass twins are allowed in the case of the single phase transition implies that, in general, two types of pairs of neutron stars could be involved in a merger event, namely, H-H, Q2-H for models with  $M_{\max}^{\text{H}} > 1.45M_{\odot}$ , and Q2-H, Q2-Q2 for EOS with  $M_{\max}^{\text{H}} < 1.35M_{\odot}$ , where H and Q2 denote hadronic and hybrid stars (with the Q2 quark phase); see Fig. 6 (a). As a general trend, the H-H combination produces the largest tidal deformabilities, the Q2-H combination produces intermediate values of tidal deformabilities, and

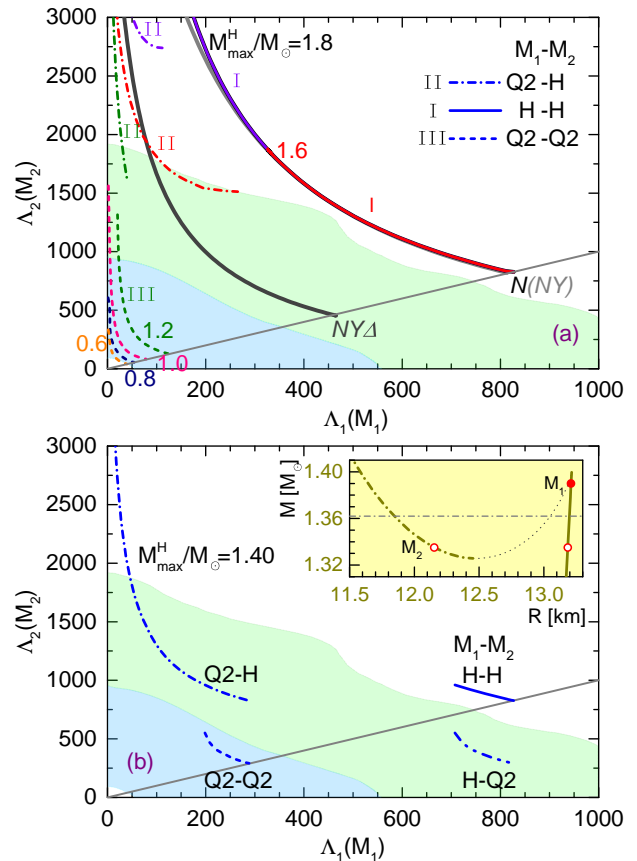


FIG. 6. (a) Tidal deformabilities of compact objects with a single phase transition for a fixed value of binary chirp mass  $\mathcal{M} = 1.186M_{\odot}$ . The EOS are labeled by the maximal mass  $M_{\max}^{\text{H}}$  of the hadronic branch of the sequences. The three types of pairs for stars with masses  $M_1$  and  $M_2$  are H-H (solid lines), Q2-H (dash-dotted lines), and Q2-Q2 (dashed lines). These three possibilities are also labeled by roman numerals I, II and III. (b) The same as in (a) but for fixed  $M_{\max}^{\text{H}} = 1.40M_{\odot}$ , which is close to the value  $M_1 = M_2 = 1.362M_{\odot}$  inferred from the GW170817 event assuming it involved equal-mass stars. The shaded regions correspond to the 50% and 90% credibility regions taken from the analysis of GW170817 within the PhenomPNRT model [48]. The inset shows the mass-radius relation around the phase transition region. The open circles (labeled  $M_2$ ) are the masses of two possible companions for the star of mass  $M_1$  (full circle) for a fixed value of binary chirp mass  $\mathcal{M} = 1.186M_{\odot}$ .

the smallest values are obtained for the Q2-Q2 combination. Since low values of tidal deformabilities are favored by the observational analysis, one may conclude that the phase transition to quark matter helps to reduce the tension between purely hadronic models and the data (see also Ref. [12]). Figure 6 also demonstrates the dependence of the results on the transition density  $\varepsilon_1$  parametrized in terms of  $M_{\max}^{\text{H}}$ : for lower phase transition density (i.e., a smaller  $M_{\max}^{\text{H}}$  value and larger quark core) the tidal deformabilities are smaller, in agreement with the fact that the stars are more compact. Furthermore, purely hadronic members can be obtained only if the transition density is high enough so that twin stars have masses heavier than  $1.362M_{\odot}$ . Interestingly, in the case where

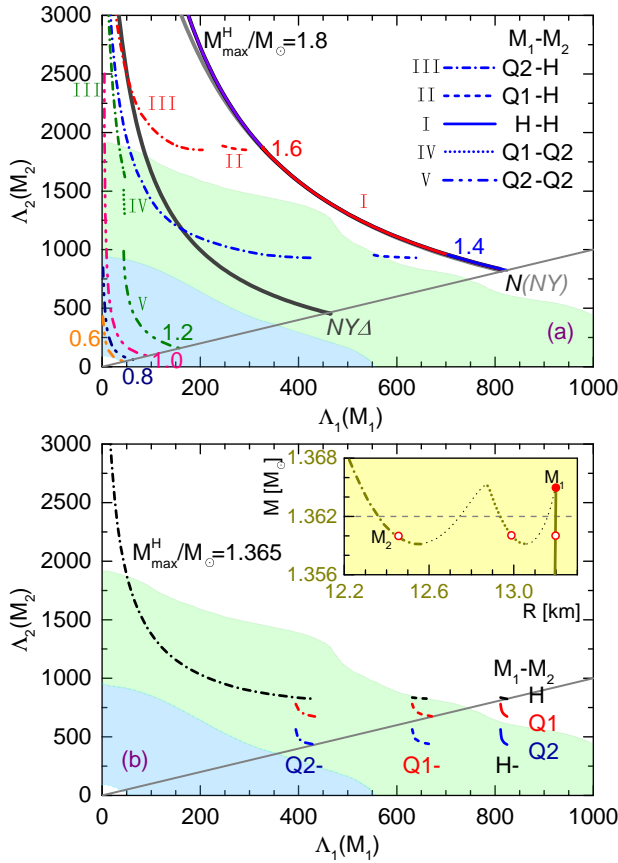


FIG. 7. The same as in Fig. 6, but in the case of two sequential phase transition (the label Q2 in the case indicates stars with two phase transitions, whereas Q1 - with a single phase transition). The distinct types of pairs of neutron stars are labeled as H-H (solid line), Q1-H (dashed line), Q2-H (dash-dotted line), Q1-Q2 (dotted line), and Q2-Q2 (dash-double-dotted line). These are also labeled by Roman numerals from I to V in the given order. Panel (b) in this case contains the following cases: (i) the primary is a Q2 star (dashed-dotted lines) with the secondary being H (black), Q1 (red), and Q2 (blue) stars; (ii) the primary is a Q1 star (dashed lines) with secondary being H (black), Q1 (red), and Q2 (blue) stars; and, finally, the primary is a hadronic star (solid lines) with the secondary being H (black), Q1 (red) and Q2 (blue) star. The inset in panel (b) shows the mass-radius relation, where the open circles correspond to masses (labeled  $M_2$ ) of the three possible companions of the primary star with mass  $M_1$  (full circle) for a fixed value of binary chirp mass  $\mathcal{M} = 1.186M_{\odot}$ .

$M_{\text{max}}^H = 1.40M_{\odot}$ , the mass twins appear around  $1.362M_{\odot}$ , as shown in the inset of Fig. 6 (b). Furthermore, an additional H-Q2 curve lies below the diagonal, which implies that for  $M_1 \geq M_2$  one has  $\Lambda_1 \geq \Lambda_2$ , which is contrary to the expectation that  $\Lambda_1 \leq \Lambda_2$ , as already observed by several authors [17–21].

If mass triplets are allowed in the case of two sequential phase transitions, there are, in general, three types of pairs of neutron stars that could be involved in a merger event, namely, H-H, Q1-H, and Q2-H for EOS with  $M_{\text{max}}^H > 1.37M_{\odot}$ , and Q2-H, Q1-Q2 and Q2-Q2 for EOS with  $M_{\text{max}}^H < 1.36M_{\odot}$ ; see Fig. 7 (a). For  $M_{\text{max}}^H = 1.365M_{\odot}$  the mass triplets arise around

$1.362M_{\odot}$ . In this case, the number of possible pairs proliferates to a total of  $3! = 6$ . Three of these are pairs of stars of the same type — H-H, Q1-Q1, and Q2-Q2 — and three are pairs of mixed type — H-Q1, H-Q2, Q1-Q2; see Fig. 7 (b). This highlights the fact that in the case of two first-order sequential phase transition it is possible to generate a rich variety of compact star mergers. In this case, we again note that three curves, namely H-Q1, H-Q2, and Q1-Q2, lie below the diagonal line in Fig. 7 (b). This is a direct extension of the effect already seen in the case of twins to the case of triplet stars.

A quantity that has been accurately measured for the GW170817 event during the inspiral phase is the mass weighted average tidal deformability  $\tilde{\Lambda}$  [52, 53], (for the measurements result, see Refs [1, 38, 48]). We show this quantity in Figs. 8 and 9 as a function of the ratio of masses  $q = M_2/M_1$  of merger components for a fixed chirp mass  $\mathcal{M} = 1.186M_{\odot}$ . The ratio  $q$  in the case of the GW170817 event was inferred to be in the range  $0.72 \leq q \leq 1$  [48, 49]. The boundaries on  $\tilde{\Lambda}$ , which were set by the gravitational-wave and electromagnetic observations, respectively, are also shown. The upper limit  $\tilde{\Lambda} = 720$  was set by the analysis of the GW170817 event (more precisely, this is the lowest value for this limit at the 90% confidence level [48]). The lower limit  $\tilde{\Lambda} \approx 250$  was deduced from the analysis of the electromagnetic counterpart of GW170817, e.g., AT2017gfo [49–51, 54]. This lower limit on  $\tilde{\Lambda}$  indicates approximately that the radius for a canonical neutron star must be larger than  $\sim 10.5$  km [50, 51].

From Figs. 8 and 9 we see that  $\tilde{\Lambda}$  weakly depends on the mass ratio  $q$  for purely hadronic EOS as well as for hybrid EOS with  $M_{\text{max}}^H < 1.0$ . For hybrid EOS with larger  $M_{\text{max}}^H$ , some variation is observed in the range of several hundreds. It is further seen that the configurations with phase transition(s), which are more compact than their nucleonic counterparts provide  $\tilde{\Lambda}$  values which are favored by the limits deduced from the GW170817 event alone. The hybrid EOS with transitional masses in the range  $1.2 \lesssim M_{\text{max}}^H/M_{\odot} \lesssim 1.6$  are

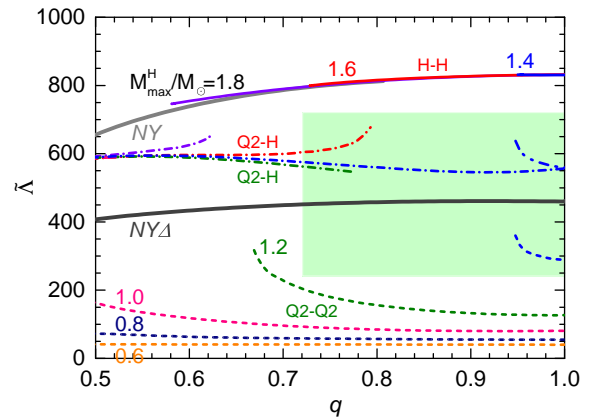


FIG. 8. Mass weighted deformability vs. mass asymmetry for a binary system with fixed chirp mass  $\mathcal{M} = 1.186M_{\odot}$  predicted by a range of hybrid EOS with a single phase transition and various values of  $M_{\text{max}}^H$ . The labeling is the same as in Fig. 6. The error shading indicates the constraints estimated from the GW170817 event [48] and the electromagnetic transient AT2017gfo [49–51].



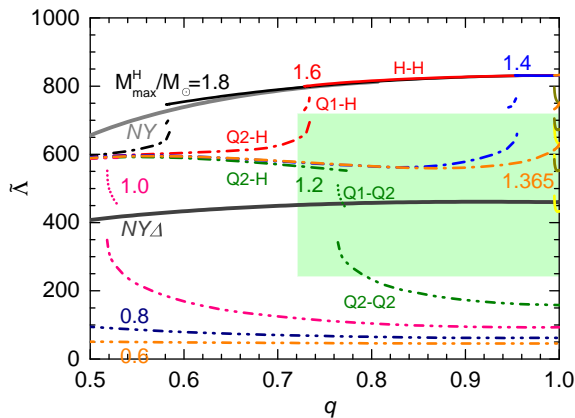


FIG. 9. The same as in Fig. 8, but in the case of EOS with two sequential phase transitions. The labeling is the same as in Fig. 7.

roughly consistent with above-mentioned limits. On the other hand, the low-mass models with  $M_{\text{max}}^H/M_{\odot} \lesssim 1.0$  can be excluded on the basis of the electromagnetic observations.

It is expected that more neutron star binary mergers will be observed within the coming years. Now, imagine comparing two such events in which the observed values of  $\Lambda_1$  are close but the  $\Lambda_2$  values are different. Such a situation may arise when the secondary star  $M_2$  has a twin or triplet configuration. Such an observation would be evidence for the existence of a strong first-order phase transition at low transition density (or mass). If, conversely, the same value for  $\Lambda_2$  but different values for  $\Lambda_1$  are observed, (i.e., two stars belonging to twin or triplet combinations with the primary star's mass  $M_1$  were merged in each event), then this would be an indication for a high transition density; see Figs. 6 and 7. Furthermore, for two events in which the observed values of chirp mass  $\mathcal{M}$  are similar but the values of mass-weighted deformabilities  $\tilde{\Lambda}$  are significantly different, such an observation also serves as a signal for the existence of (sequential) strong first-order phase transition(s); see Figs. 8 and 9.

## V. CONCLUSIONS

In this work we have explored several compositions of compact stars. On the hadronic side, we considered purely nucleonic, hypernuclear and  $\Delta$ -resonance plus hypernuclear matter. The hadronic matter was described within the density functional theory. We further assumed a first order phase transition to quark matter characterized either by a single phase or two phases. All phase transitions were assumed to be first-order and involved a density jump at the phase transition. The quark matter was described using the constant speed of sound parametrization, each phase having its own speed of sound. Starting from the EOS of these phases, we constructed the stellar models, and obtained their masses, radii and tidal deformabilities. Our results can be summarized as follows:

### (a) Variations in the hadronic envelope of the models:

We observe, consistent with the previous work, that the on-

set of hyperons allows us to keep the maximum mass of our configurations below the upper limit on the maximum mass,  $\sim 2.2M_{\odot}$ , of compact star sequences deduced from the GW170817 event. As shown previously, the inclusion of  $\Delta$ 's reduces the radii of the configuration with intermediate masses and reduces considerably the tidal deformabilities. Allowing for phase transition(s), we recover the general features known for hybrid stars, in particular, the occurrence of twin and triplet configurations. Interestingly, the low radii obtained in the case of  $\Delta$ -admixed matter exclude the appearance of stable stars with two phases of quark matter for a wide density range and, consequently, the possibility of triplets.

### (b) Conditions for the occurrence of low-mass twins/triplets:

Previous work has shown that twins are possible for masses  $M \sim 1.4M_{\odot}$  [12], while triplets were found for  $M \sim 1.7M_{\odot}$  [25]. Here we show that if the H-Q1 transition density is taken to be sufficiently low, then low-mass triplet stars can be obtained for nucleonic and hyperon- $\Delta$  admixed envelopes. For models, we produce families of stars whose maximum mass (attained on the Q2 branch) is  $2M_{\odot}$ . In doing so we assumed that the quark matter phases are characterized by stiff EOS with speeds of sound  $s_1 = 0.7$  (Q1 phase) and  $s_2 = 1$  (Q2 phase) as has been assumed in Ref. [25].

### (c) Tidal deformabilities and interpretation of GW170817:

Perhaps the most striking consequence of the existence of triplets is that the number of possible pairs that could be involved in a binary merger proliferates to 6; explicitly the pairs can now include H-H, an H-hybrid (Q1 or Q2), and a hybrid (Q2 or Q1)-hybrid (Q1 or Q2) binaries. For equal-mass binaries, all six possibilities can occur in nature, although the range of masses where this can occur is narrow. A generic conclusion, independent of the specific components of the binary, is that the emergence of quark phase(s) lifts the tension between the observations and the tidal deformabilities obtained for purely hadronic stars constructed based on relativistic density functional theory.

### (d) Inferring first-order phase transitions from observations:

The first analysis of NICER data provided values of the radius of a canonical  $M \sim 1.4M_{\odot}$  star with unprecedented accuracy [5, 6]. At the current level of accuracy these results do not contradict the radii inferred from the GW170817 event, as the values of radii extracted from both experiments have an overlap region, see Fig. 2. Should future analysis of these data or future observations result in non-overlapping regions for the radii of compact objects, this would indicate the existence of two classes of neutron stars with the same masses but substantially different radii - a hallmark of twins or triplet configurations.

Given the possibility that the LIGO-Virgo Collaboration will observe a few neutron star binary mergers during the current and next observational runs at distances of 50 to 100 Mpc, one will be in the position to compare the merger events to each other. If such events involve similar masses of primaries or secondaries with tidal deformabilities that differ significantly, beyond the bounds of experimental error, this would be an indication that different members of a twin or triplet were involved in each event. Given the strong correlation be-

tween the radii of stars and their tidal deformabilities, such observations would be complementary to the possible inferences of different radii of same-mass stars, as pointed out earlier [25]. This is potentially detectable by the NICER mission [55], which is expected to constrain the radii of several x-ray emitting neutron stars (in addition to the millisecond pulsar PSR J0030+0451) with uncertainty about 10%.

Looking ahead, the features and scenarios discussed in this work are likely to be put to the test from various sides: (a) Observations of massive pulsars in the future (for example with the Square Kilometer Array) will put further constraints on the stiffness of the EOS at high densities; (b) measurements of radii of neutron stars, such as those already obtained by the NICER experiment, will provide information on the EOS in the intermediate- to low- density range; (c) future gravitational-wave observations of neutron star-neutron star and neutron star-back hole binaries have the potential to further narrow the range of admissible EOS. Increased statistics of measurements will help to elucidate the possibility of first-order phase transitions, as manifested by the occurrence of

twins and triplets of stars.

## ACKNOWLEDGEMENTS

We thank Steven Harris, Arus Harutyunyan, Jürgen Schaffner-Bielich and Fridolin Weber for discussions. J.J.L. acknowledges the support of the Alexander von Humboldt Foundation. A.S. acknowledges the support of the DFG (Grant No. SE 1836/4-1). M.A. is supported by the U.S. Department of Energy, Office of Science, Office of Nuclear Physics under Award No. DE-FG02-05ER41375. Partial support was provided by the European COST Action “PHAROS” (CA16214) and the State of Hesse LOEWE-Program in HIC for FAIR. A.S. thanks David Blaschke and participants of the ECT\* workshop “The first compact star merger event – Implications for nuclear and particle physics” for discussions. J.J.L. is also grateful for the hospitality of Zhao-Qing Feng’s group during his stay at the South China University of Technology.

- 
- [1] B. P. Abbott, R. Abbott, T. D. Abbott, F. Acernese, K. Ackley, *et al.* (LIGO Scientific Collaboration and Virgo Collaboration), “GW170817: Observation of gravitational waves from a binary neutron star inspiral,” *Phys. Rev. Lett.* **119**, 161101 (2017).
- [2] B. P. Abbott, R. Abbott, R. X. Adhikari, A. Ananyeva, S. B. Anderson, *et al.*, “Multi-messenger observations of a binary neutron star merger,” *Astrophys. J. Lett.* **848**, L12 (2017).
- [3] B. P. Abbott, R. Abbott, T. D. Abbott, F. Acernese, K. Ackley, *et al.*, “Gravitational waves and gamma-rays from a binary neutron star merger: GW170817 and GRB170817A,” *Astrophys. J. Lett.* **848**, L13 (2017).
- [4] H. Cromartie, E. Fonseca, S. M. Ransom, P. B. Demorest, Z. Arzoumanian, *et al.*, “Relativistic Shapiro delay measurements of an extremely massive millisecond pulsar,” *Nature Astron.* **4**, 72–76 (2020).
- [5] T. E. Riley, A. L. Watts, S. Bogdanov, P. S. Ray, R. M. Ludlam, *et al.*, “A NICER view of PSR J0030+0451: Millisecond pulsar parameter estimation,” *Astrophys. J. Lett.* **887**, L21 (2019).
- [6] M. C. Miller, F. K. Lamb, A. J. Dittmann, S. Bogdanov, Z. Arzoumanian, *et al.*, “PSR J0030+0451 mass and radius from NICER data and implications for the properties of neutron star matter,” *Astrophys. J. Lett.* **887**, L24 (2019).
- [7] S. Benić, D. Blaschke, D. E. Alvarez-Castillo, T. Fischer, and S. Typel, “A new quark-hadron hybrid equation of state for astrophysics-I. High-mass twin compact stars,” *Astron. Astrophys.* **577**, A40 (2015).
- [8] M. A. R. Kaltenborn, N.-U. F. Bastian, and D. B. Blaschke, “Quark-nuclear hybrid star equation of state with excluded volume effects,” *Phys. Rev. D* **96**, 056024 (2017).
- [9] T. Fischer, N.-U. F. Bastian, M.-R. Wu, P. Baklanov, E. Sorokina, *et al.*, “Quark deconfinement as a supernova explosion engine for massive blue supergiant stars,” *Nature Astron.* **2**, 980–986 (2018).
- [10] A. Bauswein, N.-U. F. Bastian, D. B. Blaschke, K. Chatzioannou, J. A. Clark, *et al.*, “Identifying a first-order phase transition in neutron-star mergers through gravitational waves,” *Phys. Rev. Lett.* **122**, 061102 (2019).
- [11] E. Annala, T. Gorda, A. Kurkela, and A. Vuorinen, “Gravitational-wave constraints on the neutron-star-matter equation of state,” *Phys. Rev. Lett.* **120**, 172703 (2018).
- [12] V. Paschalidis, K. Yagi, D. Alvarez-Castillo, D. B. Blaschke, and A. Sedrakian, “Implications from GW170817 and I-Love-Q relations for relativistic hybrid stars,” *Phys. Rev. D* **97**, 084038 (2018).
- [13] R. Nandi and P. Char, “Hybrid stars in the light of GW170817,” *Astrophys. J.* **857**, 12 (2018).
- [14] E. R. Most, L. R. Weih, L. Rezzolla, and J. Schaffner-Bielich, “New constraints on radii and tidal deformabilities of neutron stars from GW170817,” *Phys. Rev. Lett.* **120**, 261103 (2018).
- [15] I. Tews, J. Margueron, and S. Reddy, “Critical examination of constraints on the equation of state of dense matter obtained from GW170817,” *Phys. Rev. C* **98**, 045804 (2018).
- [16] G. F. Burgio, A. Drago, G. Pagliara, H.-J. Schulze, and J.-B. Wei, “Are small radii of compact stars ruled out by GW170817/AT2017gfo?” *Astrophys. J.* **860**, 139 (2018).
- [17] D. E. Alvarez-Castillo, D. B. Blaschke, A. G. Grunfeld, and V. P. Paura, “Third family of compact stars within a nonlocal chiral quark model equation of state,” *Phys. Rev. D* **99**, 063010 (2019).
- [18] J.-E. Christian, A. Zacchi, and J. Schaffner-Bielich, “Signals in the tidal deformability for phase transitions in compact stars with constraints from GW170817,” *Phys. Rev. D* **99**, 023009 (2019).
- [19] S. Han and A. W. Steiner, “Tidal deformability with sharp phase transitions in binary neutron stars,” *Phys. Rev. D* **99**, 083014 (2019).
- [20] G. Montaña, L. Tolós, M. Hanauske, and L. Rezzolla, “Constraining twin stars with GW170817,” *Phys. Rev. D* **99**, 103009 (2019).
- [21] M. Sieniawska, W. Turczański, M. Bejger, and J. L. Zdunik, “Tidal deformability and other global parameters of compact stars with strong phase transitions,” *Astron. Astrophys.* **622**, A174 (2019).
- [22] R. Essick, P. Landry, and D. E. Holz, “Nonparametric inference of neutron star composition, equation of state, and maximum

- mass with GW170817,” *Phys. Rev. D* **101**, 063007 (2020).
- [23] J. J. Li and A. Sedrakian, “Implications from GW170817 for  $\Delta$ -isobar admixed hypernuclear compact stars,” *Astrophys. J. Lett.* **874**, L22 (2019).
- [24] J. J. Li and A. Sedrakian, “Constraining compact star properties with nuclear saturation parameters,” *Phys. Rev. C* **100**, 015809 (2019).
- [25] M. Alford and A. Sedrakian, “Compact stars with sequential QCD phase transitions,” *Phys. Rev. Lett.* **119**, 161104 (2017).
- [26] D. Bailin and A. Love, “Superfluidity and superconductivity in relativistic fermion systems,” *Phys. Rep.* **107**, 325–385 (1984).
- [27] M. Alford, K. Rajagopal, and F. Wilczek, “Color-flavor locking and chiral symmetry breaking in high density QCD,” *Nucl. Phys. B* **537**, 443–458 (1999).
- [28] L. Bonanno and A. Sedrakian, “Composition and stability of hybrid stars with hyperons and quark color-superconductivity,” *Astron. Astrophys.* **539**, A16 (2012).
- [29] G. A. Lalazissis, T. Nikšić, D. Vretenar, and P. Ring, “New relativistic mean-field interaction with density-dependent meson-nucleon couplings,” *Phys. Rev. C* **71**, 024312 (2005).
- [30] J. J. Li, A. Sedrakian, and F. Weber, “Competition between delta isobars and hyperons and properties of compact stars,” *Phys. Lett. B* **783**, 234–240 (2018).
- [31] J. L. Zdunik and P. Haensel, “Maximum mass of neutron stars and strange neutron-star cores,” *Astron. Astrophys.* **551**, A61 (2013).
- [32] M. G. Alford, S. Han, and M. Prakash, “Generic conditions for stable hybrid stars,” *Phys. Rev. D* **88**, 083013 (2013).
- [33] M. Alford, K. Rajagopal, S. Reddy, and F. Wilczek, “Minimal color-flavor-locked–nuclear interface,” *Phys. Rev. D* **64**, 074017 (2001).
- [34] L. F. Palhares and E. S. Fraga, “Droplets in the cold and dense linear sigma model with quarks,” *Phys. Rev. D* **82**, 125018 (2010).
- [35] P. B. Demorest, T. Pennucci, S. M. Ransom, M. S. E. Roberts, and J. W. T. Hessels, “A two-solar-mass neutron star measured using Shapiro delay,” *Nature* **467**, 1081 (2010).
- [36] J. Antoniadis, P. C. C. Freire, N. Wex, T. M. Tauris, R. S. Lynch, *et al.*, “A massive pulsar in a compact relativistic binary,” *Science* **340**, 1233232 (2013).
- [37] E. Fonseca, T. T. Pennucci, J. A. Ellis, I. H. Stairs, D. J. Nice, *et al.*, “The NANOGrav nine-year data set: Mass and geometric measurements of binary millisecond pulsars,” *Astrophys. J.* **832**, 167 (2016).
- [38] B. P. Abbott, R. Abbott, T. D. Abbott, F. Acernese, K. Ackley, *et al.* (The LIGO Scientific Collaboration and the Virgo Collaboration), “GW170817: Measurements of neutron star radii and equation of state,” *Phys. Rev. Lett.* **121**, 161101 (2018).
- [39] B. Margalit and B. D. Metzger, “Constraining the maximum mass of neutron stars from multi-messenger observations of GW170817,” *Astrophys. J. Lett.* **850**, L19 (2017).
- [40] M. Shibata, S. Fujibayashi, K. Hotokezaka, K. Kiuchi, K. Kyutoku, Y. Sekiguchi, and M. Tanaka, “Modeling GW170817 based on numerical relativity and its implications,” *Phys. Rev. D* **96**, 123012 (2017).
- [41] M. Ruiz, S. L. Shapiro, and A. Tsokaros, “GW170817, general relativistic magnetohydrodynamic simulations, and the neutron star maximum mass,” *Phys. Rev. D* **97**, 021501 (2018).
- [42] L. Rezzolla, E. R. Most, and L. R. Weih, “Using gravitational-wave observations and quasi-universal relations to constrain the maximum mass of neutron stars,” *Astrophys. J. Lett.* **852**, L25 (2018).
- [43] R. Schaeffer, L. Zdunik, and P. Haensel, “Phase transitions in stellar cores. I. equilibrium configurations,” *Astro. Astrophys.* **126**, 121–145 (1983).
- [44] F. Özel and P. Freire, “Masses, radii, and the equation of state of neutron stars,” *Ann. Rev. Astro. Astrophys.* **54**, 401–440 (2016).
- [45] G. Colucci and A. Sedrakian, “Equation of state of hypernuclear matter: Impact of hyperon-scalar-meson couplings,” *Phys. Rev. C* **87**, 055806 (2013).
- [46] M. Oertel, C. Providência, F. Gulminelli, and Ad. R. Raduta, “Hyperons in neutron star matter within relativistic mean-field models,” *J. Phys. G.* **42**, 075202 (2015).
- [47] J. J. Li, W. H. Long, and A. Sedrakian, “Hypernuclear stars from relativistic Hartree-Fock density functional theory,” *Eur. Phys. J. A* **54**, 133 (2018).
- [48] B. P. Abbott, R. Abbott, T. D. Abbott, F. Acernese, K. Ackley, *et al.* (LIGO Scientific Collaboration and Virgo Collaboration), “Properties of the binary neutron star merger GW170817,” *Phys. Rev. X* **9**, 011001 (2019).
- [49] M. W. Coughlin, T. Dietrich, Z. Doctor, D. Kasen, S. Coughlin, *et al.*, “Constraints on the neutron star equation of state from AT2017gfo using radiative transfer simulations,” *Mon. Not. Roy. Astron. Soc.* **480**, 3871 (2018).
- [50] D. Radice and L. Dai, “Multimessenger parameter estimation of GW170817,” *Eur. Phys. J. A* **55**, 50 (2019).
- [51] K. Kiuchi, K. Kyutoku, M. Shibata, and K. Taniguchi, “Revisiting the lower bound on tidal deformability derived by AT2017gfo,” *Astrophys. J. Lett.* **876**, L31 (2019).
- [52] T. Hinderer, B. D. Lackey, R. N. Lang, and J. S. Read, “Tidal deformability of neutron stars with realistic equations of state and their gravitational wave signatures in binary inspiral,” *Phys. Rev. D* **81**, 123016 (2010).
- [53] L. Wade, J. D. E. Creighton, E. Ochsner, B. D. Lackey, B. F. Farr, *et al.*, “Systematic and statistical errors in a Bayesian approach to the estimation of the neutron-star equation of state using advanced gravitational wave detectors,” *Phys. Rev. D* **89**, 103012 (2014).
- [54] D. Radice, A. Perego, F. Zappa, and S. Bernuzzi, “GW170817: Joint constraint on the neutron star equation of state from multimessenger observations,” *Astrophys. J. Lett.* **852**, L29 (2018).
- [55] K. C. Gendreau, Z. Arzumanyan, P. W. Adkins, C. L. Albert, J. F. Anders, *et al.*, “The neutron star interior composition explorer (NICER): design and development,” in *Space Telescopes and Instrumentation 2016: Ultraviolet to Gamma Ray*, Vol. 9905 (2016) p. 99051H.